Analysis of a new front-end structure offset impact: mass-spring-damper models with piecewise linear characteristics

Ahmed Elmarakbi

Department of Computing, Engineering and Technology,
Faculty of Applied Sciences,
University of Sunderland,
St. Peter's Campus, Sunderland SR6 0DD, UK
E-mail: ahmed.elmarakbi@sunderland.ac.uk

Abstract: In this paper, new front-end structures (smart) are proposed to improve vehicle frontal impact. The work carried out in this paper includes developing and analysing mathematical models of vehicle-to-rigid barrier offset frontal impact using fixed and extendable smart front-end structures with piecewise linear characteristics. In these models, vehicle components are modelled by lumped masses and non-linear springs. Moreover, the hydraulic cylinders are represented by non-linear damper elements. In this paper, the dynamic responses of the crash events are obtained with the aid of analytical approach using incremental harmonic balance method. In addition, the intrusion injury and occupant deceleration are used for interpreting the results. It is demonstrated from simulation results that significant improvements to both intrusion and deceleration injuries are obtained using the smart front-end structures.

Keywords: crashworthiness; vehicle-to-rigid offset frontal impact; smart front-end structures; incremental harmonic balance method; IHB.

Reference to this paper should be made as follows: Elmarakbi, A. (2010) 'Analysis of a new front-end structure offset impact: mass-spring-damper models with piecewise linear characteristics', *Int. J. Vehicle Systems Modelling and Testing*, Vol. 5, No. 4, pp.292–311.

Biographical notes: Ahmed Elmarakbi is a Senior Lecturer of Automotive Engineering at University of Sunderland. He leads an enthusiastic, expanding group of currently five PhD students. His research interests lie in the area of vehicle crashworthiness and safety, energy efficient vehicles, electrical vehicles, low carbon vehicles, composites and lightweight materials. His research outcomes are recognised both nationally and internationally as evident from his over 70 publications. He received many prestigious awards and grants (over a million €), including JSPS Japan, NSERC Canada and EPSRC UK.

1 Introduction

Accident analyses have shown that two-thirds of the collisions in which car occupants have been injured are frontal collisions (Hobbes, 1991; Mizuno et al., 1997). Despite worldwide advances in research programs to develop intelligent safety systems, frontal

Copyright © 2010 Inderscience Enterprises Ltd.

collision remains the major source of road fatalities and serious injuries for decades to come (Hiroyuki, 1990). The evaluation of the deformation behaviour of the front-end of passenger vehicles has been based on the assumption that in frontal collisions, the kinetic energy of the vehicle should be transformed into plastic deformation with a minimum deformation of the vehicle (Elsholz, 1974).

The majority of real world frontal impacts involve partial overlap collision. The problem is that the same amount of energy must be absorbed either with a single, or with both longitudinal members (rails). This problem cannot be solved by just increasing the stiffness of the rails in such a way that each rail is capable of absorbing all of the crash energy. Due to the physical nature of the offset frontal collision event, only one of the two longitudinal rails contributes toward the energy absorption. This leads to undesirable intrusions in the passenger compartment. Excessive intrusion is usually generated on the impacted side subjecting occupants to injury risks. These injuries are more severe than the injuries generated during full frontal collision. A trade-off between excessive intrusion and smooth deceleration of occupants is the most difficult problem to be satisfied when designing for an offset crash event. In addition, compatibility of large vehicles in head-on collision with small vehicles requires the front-end structure to protect its occupant, as well as the occupants of the smaller vehicles. Due to the aggressive design of the large vehicles involved in a collision with smaller vehicle, the protection of the occupant of both small and large vehicles are conflicting each other. Only the large vehicle contributes toward its occupant protection. This leads to undesirable intrusions in the passenger compartment of the small vehicle. The trade-off and compatibility problems make it more challenging to seek an optimal design that maximises the energy absorption capability of the crash zones, minimises intrusion, and keeps occupant's deceleration within acceptable limits.

A new direction of crashworthiness improvement using smart front-end structures is introduced to support the function of the existing vehicle structure. This paper seeks to develop mathematical models of the smart structure in different impact situations and to find analytical solutions to these models. A review of the previous work shows that little has been done for developing simplified models for automotive crash problems in general and smart structures in particular. The development of such models is desirable to be used in the initial concept design stage of automotive structures. Using these simplified models, it is possible to perform a rapid analysis for the structure.

2 New front-end structures

2.1 Proposed types of smart front-end structures

There are two types of smart front-end structures proposed to improve the vehicle crashworthiness. The first type consists of two non-extendable (fixed) hydraulic cylinders

parallel to the longitudinal members as shown in Figure 1(a). The second type consists of two extendable controlled hydraulic cylinders integrated with the front-end longitudinal members as shown in Figure 1(b).

Figure 1 Two types of smart front-end structures (a) fixed smart front-end structure (b) extendable smart front-end structure

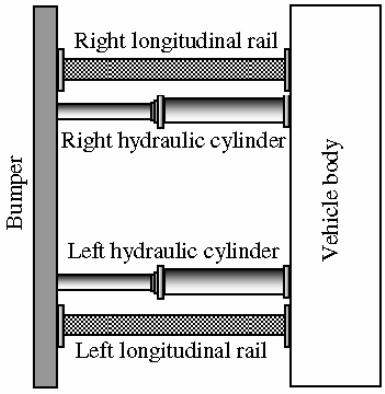

(a)

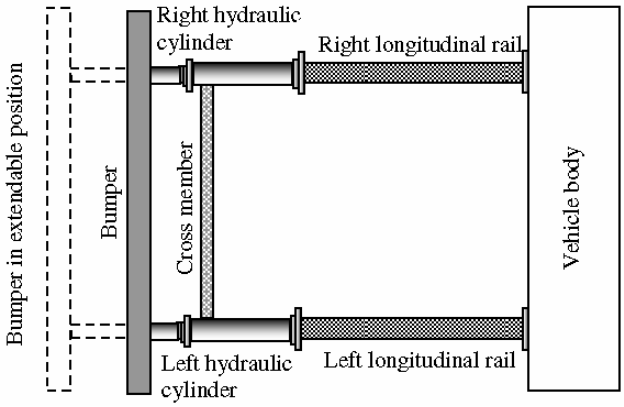

(b)

Frontal crashworthiness improvement using hydraulic cylinders was initially developed by Schwarz (1971). In his research, hydraulic energy absorption systems were designed to mitigate high speed impacts up to 80 km/h. Moreover, using hydraulic cylinders to absorb crash energy at high speed collisions was investigated by Appel and Tomasd (1973) to improve the crashworthiness of motor vehicles. The basic idea was tested by Rupp (1974). In his research, he utilised hydraulic buffers to maximise the absorbed impact energy. He adopted two extendable, independently controlled hydraulic buffers integrated with the front-end longitudinal members. Rupp's study aimed at mitigating high-speed frontal impacts. Five different strokes were used and different impact speeds were investigated ranging from 36 km/h to 73 km/h. Recently, Jawad and Baccouch

(2001) and Jawad el al. (1999) used hydraulic cylinders to mitigate high speed frontal impact. In their works, two controlled hydraulic cylinders were proposed to be extended prior to collision and absorb impact energy upon engagement with the other colliding body using radar collision prediction sensors.

Moreover, high speed collisions at 36 km/h, 56 km/h and 64 km/h were investigated in their research. Furthermore, Witteman and Kriens (1998, 2001) used non-extendable hydraulic cylinders to improve the frontal impact at initial crash speed of 56 km/h. In addition, Witteman (1999) presented a study showing that increased protection for the entire collision spectrum can be obtained by a frontal structure consisting of two special longitudinal members. The longitudinal members are supported by a cable connection system for symmetric force distribution. Similar research by Clark (1994) presented another solution to improve vehicle frontal crashworthiness and to reduce the crash severity. In his work, he developed an extended airbag bumper system, in which a radar detection sensor detects the collision and a large airbag deploys in front of the bumper.

In automotive industry, safety engineers continue their efforts in development of smart structures. There are a few patents on smart structures since 1976 invented by Ellis (1976), Reuber and Braun (1994), Wang (1994), and Namuduri et al. (2004) on the design procedures. However, there is a lack of research with regard to the analysis of smart structures.

In the following sections, mathematical models of the smart front-end structures in offset frontal barrier impact will be developed and analytical solutions to these models will be presented for crashworthiness study.

2.2 Mass-spring-damper models

In this section, mathematical models and associated equations of motion are developed to predict the dynamic response of vehicle crash. In these models, the deformation parts representing the longitudinal rails are defined by spring elements with piecewise linear characteristics as an approximation of a real force-deformation curve. The hydraulic cylinders are also represented by piecewise linear damper elements as an approximation of a real force-velocity curve. The vehicle body, cross member, bumper and occupant are defined by lumped masses. The occupant-restraint system is represented by stiffness and damper elements.

The lumped-mass model shown in Figure 2 represents a standard vehicle-to-barrier offset frontal impact. Moreover, the lumped-mass models represent a smart vehicle-to-barrier offset frontal impact for fixed and extendable smart front-end structures are depicted in Figure 3 and Figure 4, respectively.

The initial velocity of impact is v_0. The stiffness elements shown as springs with stiffness k_i are the plastic deformation parts representing the longitudinal rails. The hydraulic cylinders are represented by dampers with damping coefficients c_k. The mass and the mass moment of inertia of the bumper are defined by m_b and I_b, respectively. Moreover, the mass and the mass moment of inertia of the cross member are defined by m_C and I_C, respectively. In addition, the occupant – restraint characteristics of seat belt and airbag are represented by stiffness k_o and damping coefficient c_o. The masses of the passenger compartment and the occupant are represented by M, and m_o, respectively.

Figure 2 Standard vehicle-to-rigid barrier offset frontal impact (see online version for colours)

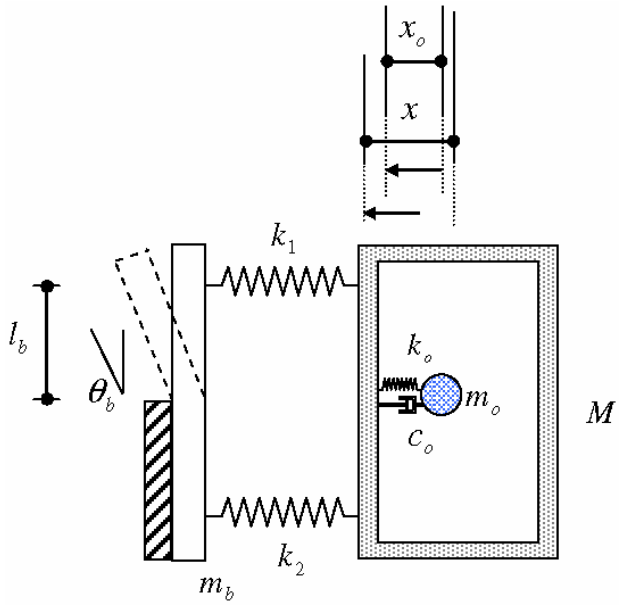

Figure 3 Fixed smart front-end structure-to-rigid barrier offset frontal impact (see online version for colours)

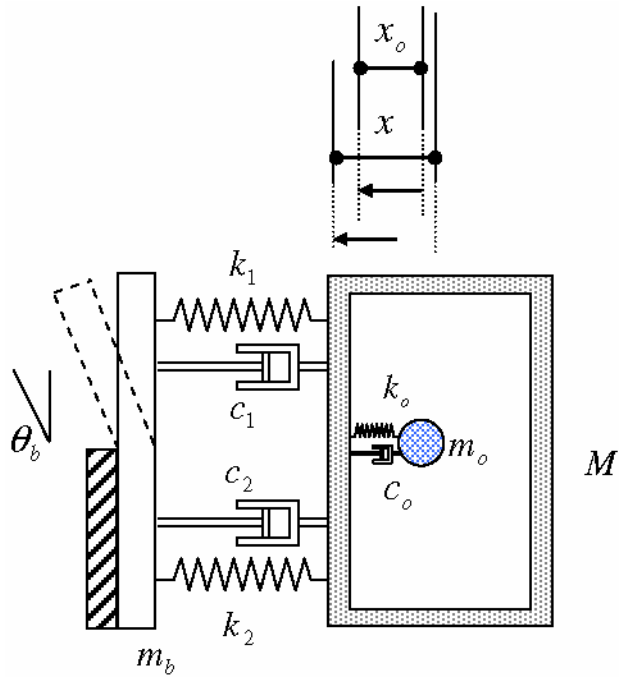

Figure 4 Extendable smart front-end structure-to-rigid barrier offset frontal impact (see online version for colours)

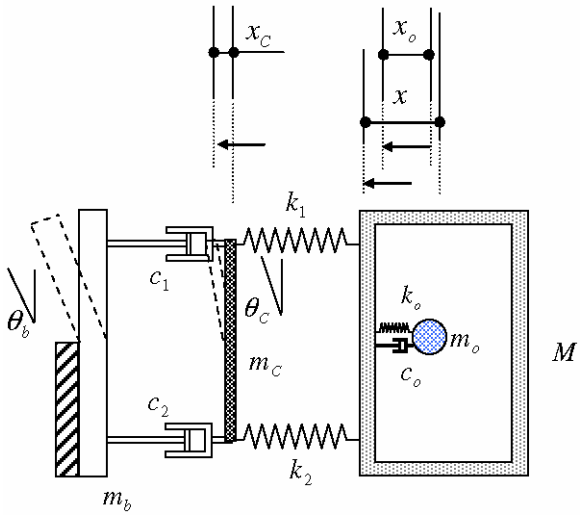

2.3 Force models

In this paper, the forces of the plastic springs $F_{si}(\delta_i)$, Figure 5, are defined as a piecewise function in the displacement domain as follows:

$$F_{si} = f_{0i} + k_i.\delta_i - F_{0i} \tag{1.a}$$

where

$$k_i = k_{i1}, \quad F_{0i} = 0 \qquad \delta_i \le \delta_i^* \tag{1.b}$$

$$k_i = k_{i2}, \quad F_{0i} = \left(k_{i2} - k_{i1}\right).\delta_i^* \qquad \delta_i > \delta_i^* \tag{1.c}$$

i = 1, 2 (i = 1 represents the right longitudinal rail, and i = 2 represents the left longitudinal rail).

The damping forces generated by the hydraulic cylinders $F_{dk}(v_{dk})$ as an additional energy absorption system are also expresses using a piecewise function in the velocity domain, Figure 6, as follows:

$$F_{dk} = c_k.v_{dk} - F_{dk} \tag{2.a}$$

where

$$c_k = c_{k1}, \quad F_{dk} = 0 \qquad v_{kd} \le v_{dk}^* \tag{2.b}$$

$$c_k = c_{k2}, \quad F_{dk} = \left(c_{k2} - c_{k1}\right).v_{dk}^* \qquad v_{kd} > v_{dk}^* \tag{2.c}$$

where k = 1, 2 (k =1 represents the right cylinder, k = 2 represents the left cylinder).

During a frontal collision, the impact force generated between obstacle and vehicle induces a sudden deceleration of the vehicle structure. The occupant safety restraint

systems such as the seat belt and airbag define the interaction between occupant body and vehicle structure. Moreover, restraint systems limit occupant's motion and mitigate injuries that may result from contact with the vehicle interior during sudden deceleration conditions. For the protection of occupants in crash, regulatory agencies specify the vehicle crashworthiness requirements in terms of force and deceleration experienced by the occupant's body parts. The force generated on the occupant by the spring $F_{so}(\delta_o)$, Figure 7, is defined as follows:

$$F_{so} = k.(\delta_o - \delta_{oc}) \tag{3.a}$$

where

$$k = 0 \qquad \delta_o \le \delta_{oc} \tag{3.b}$$

$$k = k_o \qquad \delta_o > \delta_{oc} \tag{3.c}$$

Moreover, the damping force of the occupant $F_{do}(v_o)$ is determined as

$$F_{do} = c.(v_o - v_{oc}) \tag{4.a}$$

where

$$c = 0 \qquad v_o \le v_{oc} \tag{4.b}$$

$$c = c_o \qquad v_o > v_{oc} \tag{4.c}$$

where δ_{oc} is the initial slack length. The slack length represents the relative displacement of the occupant δ_o before the seatbelt becomes effective. The relative velocity of the occupant when the seatbelt becomes effective is defined by v_{oc}.

Figure 5 Force-deformation characteristics

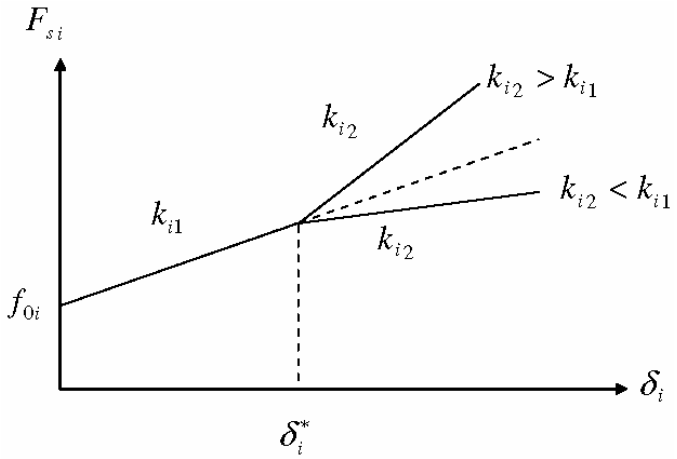

Note: Piecewise linear characteristics.

Figure 6 Force-velocity characteristics

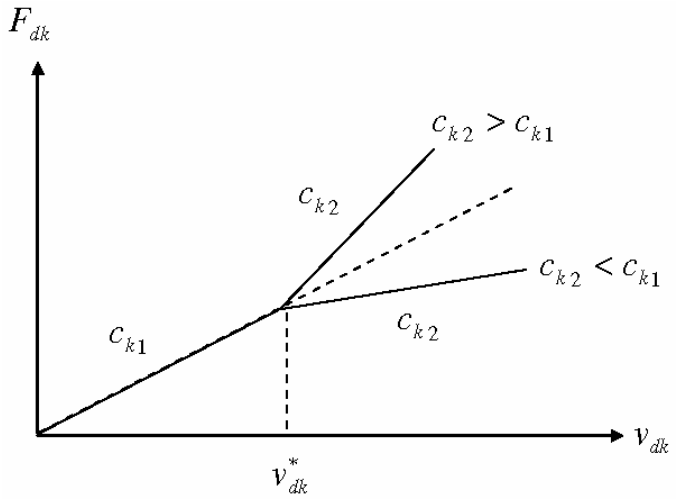

Note: Piecewise linear characteristics.

Figure 7 Force-deformation characteristic of the occupant

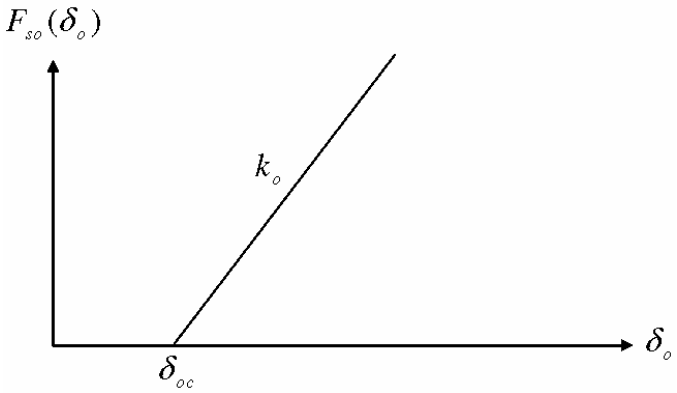

3 Solution to vehicle/barrier offset frontal impact

The goal of this section is to analyse vehicle crashworthiness and to find the dynamic response; deformation and declaration, of the vehicle and the occupant involved in barrier offset frontal impact. Analysis of a vehicle in a frontal crash event, in general, consists of studies of the vehicle response and the occupant response. Basically, there are two stages in a vehicle frontal impact with a fixed barrier: the primary and the secondary impacts. The primary impact is the collision between the vehicle front-end structure and an obstacle (barrier). The secondary impact is between the occupant and the restraint system and/or the vehicle interior. In the following sections, the primary and the secondary impacts are analysed and analytical solutions for the mathematical models are presented for fixed and extendable front-end structures, respectively.

3.1 Primary impact of the fixed smart front-end structure

To predict the behaviour of a vehicle with the fixed smart front-end structure involved in a head-on collision with a rigid barrier, the mathematical model shown in Figure 3 is used to obtain the dynamic response of both standard and smart vehicles. The following equations of motion are developed as

$$M.\ddot{x} + F_{s1}(\delta_1) + F_{s2}(\delta_2) + F_{d1}(v_{d1}) + F_{d2}(v_{d2}) = 0 \tag{5}$$

$$I_b.\ddot{\theta}_b - \left[F_{d1}(v_{d1}) + F_{s1}(\delta_1)\right].l_b = 0 \tag{6}$$

where $\ddot{x}$ is the translation deceleration of the vehicle body. $\ddot{\theta}_b$ and I_b are the rotational decelerations and masses moment of inertia of the bumper assembly, respectively. $F_{si}(\delta_i)$ and $F_{dk}(v_{dk})$ are the forces of the plastic springs and damping forces, respectively.

The deformations of the plastic springs are given by

$$\delta_1 = x - x_1, \delta_2 = x - x_2 \tag{7}$$

The velocities of the hydraulic cylinders are defined as

$$v_{d1} = \dot{x} - \dot{x}_1, v_{d2} = \dot{x} - \dot{x}_2 \tag{8}$$

The displacements of the springs' ends x_1 and x_2 are defined as follows:

$$x_1 = l_b.\tan\theta_b, x_2 = 0 \tag{9}$$

and the velocities of the dampers ends are given by

$$\dot{x}_1 = l_b.\sec^2\theta_b\dot{\theta}_b, \dot{x}_2 = 0 \tag{10}$$

Substituting equations (1), (2), (7) to (10) into equations (5) and (6) yields

$$M\ \ddot{x} + k_1.(x - l_b.\tan\theta_b) + k_2.x + c_1.(\dot{x} - l_b.\sec^2\theta_b\dot{\theta}_b) + c_2.\dot{x} = F_1 \tag{11}$$

$$I_b.\ddot{\theta}_b - c_1.(\dot{x} - l_b.\sec^2\theta_b\dot{\theta}_b)l_b - k_1.(x - l_b.\tan\theta_b)l_b = F_2 \tag{12}$$

Equations (11) and (12) can be rewritten in matrix the form as

$$\mathbf{M}.\ddot{\mathbf{x}} + (\mathbf{C_L} + \mathbf{C_{NL}})\cdot\dot{\mathbf{x}} + (\mathbf{K_L} + \mathbf{K_{NL}})\cdot\mathbf{x} = \mathbf{F} \tag{13}$$

where $\ddot{\mathbf{x}}, \dot{\mathbf{x}}$, and $\mathbf{x}$ are the $N \times 1$ acceleration, velocity and displacement vectors, respectively. N is the number of degree of freedoms for the models in Figure 2 to Figure 4. $\mathbf{M}$, $\mathbf{C_L}$, $\mathbf{C_{NL}}$, $\mathbf{K_L}$, $\mathbf{K_{NL}}$, $\mathbf{F}$ are mass, linear damping, cubic non-linear damping, linear stiffness, cubic non-linear stiffness and force matrices, respectively, and are given as following.

$$\begin{aligned}
&\mathbf{C_L} = \begin{bmatrix} c_1 + c_2 & 0 \\ -c_1.l_b & 0 \end{bmatrix},\ \mathbf{C_{NL}} = \begin{bmatrix} 0 & -c_1.l_b.(S\theta)_b \\ 0 & c_1.l_b.(S\theta)_b \end{bmatrix},\ \mathbf{K_L} = \begin{bmatrix} k_1 + k_2 & 0 \\ -k_1.l_b & 0 \end{bmatrix}, \\
&\mathbf{K_{NL}} = \begin{bmatrix} 0 & -k_1.l_b.\bar{\theta}_b \\ 0 & k_1.l_b.\bar{\theta}_b \end{bmatrix} \text{ and } \mathbf{F} = \begin{bmatrix} F_{01} + F_{02} - f_{01} - f_{02} + F_{d1} + F_{d2} \\ (f_{01} - f_{02} - F_{d1}).l_b \end{bmatrix}
\end{aligned} \tag{14}$$

where

$$\bar{\theta}_b = \left(1 + \frac{\theta_b^2}{3} + \frac{2\theta_b^4}{15} + ...\right) \tag{15}$$

$$(S\theta)_b = \sec^2\left(\theta_b\right) = \left(1 + \theta_b^2 + \frac{2\theta_b^4}{3} + \frac{17\theta_b^6}{45} + ...\right) \tag{16}$$

There is no known general solution of the non-linear equation of motion in equation (13). The purpose of this section is to describe a method that can be used to find the analytical solution of equation (13).

One of the most popular methods for approximating the solutions of equation (13) is known as incremental harmonic balance (IHB) method. The IHB method was developed by Lau et al. (1982). The IHB method was successfully applied to various types of non-linear structural systems. Although it is valid for multi-degree-of-freedoms, the applications of this method were limited to study the steady state response with two degree-of-freedom system. Moreover, only non-linear stiffness characteristics have been considered in the work of Lau et al. (1982, 1983, 1984, 1989), Lau and Zhang (1992), Lau and Yuen (1993), Pun and Liu (2000), and Chen et al. (2001).

The extensions of the present method are done in this research by adding the expression $\mathbf{C_{NL}}$ in equation (13) entering non-linear damping term and adding the large rotation term (θ) in the non-linear stiffness matrix 'offset impact'. Moreover, the method is used to solve multi-degree of freedom systems for different collision events.

To apply the IHB method, first define N time variables:

$$\tau_m = \omega_m t \ \ (m = 1, 2, ..., N) \tag{17}$$

Further, two differential operators are defined:

$$\frac{d}{dt} = \sum_{m=1}^{N} \omega_m \frac{\partial}{\partial \tau_m}, \frac{d^2}{dt^2} = \sum_{m=1}^{N}\sum_{n=1}^{N} \omega_m \omega_n \frac{\partial^2}{\partial \tau_m \partial \tau_n} \tag{18}$$

By using equations (17) and (18), equation (13) can be rewritten in the form:

$$\sum_{m=1}^{N} \omega_m \left(\sum_{n=1}^{N} \omega_n \mathbf{M} \frac{\partial^2 \mathbf{x}}{\partial \tau_m \partial \tau_n} + \left[\mathbf{C_L} + \mathbf{C_{NL}} \left(\omega_m \frac{\partial \mathbf{x}}{\partial \tau_m} \right) \right] \frac{\partial \mathbf{x}}{\partial \tau_m} \right) + \mathbf{K_L} + \mathbf{K_{NL}}(\mathbf{x}).\mathbf{x} = 0 \tag{19}$$

As a first step of the IHB method, apply the Newoton-Raphson iterative procedure by expressing the current solutions $\mathbf{x}_{new}$, $(\omega_m)_{new}$ as the sum of the previous solutions $\mathbf{x}$, ω_m and the solution increments $\Delta\mathbf{x}$, $\Delta\omega_m$ as

$$\mathbf{x}_{new} = \mathbf{x} + \Delta\mathbf{x} \tag{20}$$

$$\left(\omega_m\right)_{new} \omega_m + \Delta\omega_m \tag{21}$$

Equation (19) can be rewritten using equations (20) and (21) as

$$\sum_{m=1}^{N}(\omega_m+\Delta\omega_m)\left(\sum_{n=1}^{N}(\omega_n+\Delta\omega_n)\mathbf{M}\frac{\partial^2(\mathbf{x}+\Delta\mathbf{x})}{\partial\tau_m\partial\tau_n}\right.$$
$$+\left[\mathbf{C_L}+\mathbf{C_{NL}}\left((\omega_m+\Delta\omega_m)\frac{\partial(\mathbf{x}+\Delta\mathbf{x})}{\partial\tau_m}\right)\right]\left.\frac{\partial(\mathbf{x}+\Delta\mathbf{x})}{\partial\tau_m}\right) \tag{22}$$
$$+\left[\mathbf{K_L}+\mathbf{K_{NL}}(\mathbf{x}+\Delta\mathbf{x})\right](\mathbf{x}+\Delta\mathbf{x})=0$$

The non-linear matrix differential equation (22) can be linearised by expanding its terms in Taylor series about its initial solution, keeping only linear terms of increments in the series expansion:

$$\sum_{m=1}^{N}\omega_m\left(\sum_{n=1}^{N}\omega_n\mathbf{M}\frac{\partial^2\Delta\mathbf{x}}{\partial\tau_m\partial\tau_n}+\left[\mathbf{C_L}+\frac{\partial}{\partial\dot{\mathbf{x}}}\right]\left[\mathbf{C_{NL}}\left(\omega_m\frac{\partial\mathbf{x}}{\partial\tau_m}\right)\cdot\frac{\partial\mathbf{x}}{\partial\tau_m}\right]\frac{\partial\Delta\mathbf{x}}{\partial\tau_m}\right)$$
$$+\left[\mathbf{K_L}+\frac{\partial}{\partial\mathbf{x}}\left[\mathbf{K_{NL}}(\mathbf{x}).\mathbf{x}\right]\right]\Delta\mathbf{x}$$
$$=-\sum_{m=1}^{N}\omega_m\left(\sum_{n=1}^{N}\omega_n\mathbf{M}\frac{\partial^2\Delta\mathbf{x}}{\partial\tau_m\partial\tau_n}+\left[\mathbf{C_L}+\mathbf{C_{NL}}\left(\omega_m\frac{\partial\mathbf{x}}{\partial\tau_m}\right)\right]\frac{\partial\mathbf{x}}{\partial\tau_m}\right)-\left[\mathbf{K_L}+\mathbf{K_{NL}}(\mathbf{x})\right].\mathbf{x} \tag{23}$$
$$-\sum_{m=1}^{N}\Delta\omega_m\left(\sum_{n=1}^{N}2\omega_n\mathbf{M}\frac{\partial^2\Delta\mathbf{x}}{\partial\tau_m\partial\tau_n}+\mathbf{C_L}\cdot\left(\frac{\partial\mathbf{x}}{\partial\tau_m}\right)+\frac{\partial}{\partial\omega_m}\left[\mathbf{C_{NL}}\left(\omega_m\frac{\partial\mathbf{x}}{\partial\tau_m}\right)\cdot\omega_m\frac{\partial\mathbf{x}}{\partial\tau_m}\right]\right)$$

Equation (23) is a linear matrix differential equation in terms of unknown vector $\Delta\mathbf{x}$, which represents the increments of vector $\mathbf{x}$ in the Newton-Raphson iterative procedure. The initial solution of vector $\mathbf{x}$ and its increment $\Delta\mathbf{x}$ can be assumed by the following equation:

$$\mathbf{x}=\mathbf{H}\mathbf{z},\Delta\mathbf{x}=\mathbf{H}\Delta\mathbf{z} \tag{24}$$

where

$$\mathbf{H}=\begin{bmatrix}\mathbf{h}&0&\dots&0\\0&\mathbf{h}&\dots&0\\\vdots&\vdots&\ddots&\vdots\\0&0&\dots&\mathbf{h}\end{bmatrix},\ \mathbf{z}=\begin{bmatrix}\mathbf{z}_1\\\mathbf{z}_2\\\vdots\\\mathbf{z_N}\end{bmatrix},\ \text{and}\ \Delta\mathbf{z}=\begin{bmatrix}\Delta\mathbf{z}_1\\\Delta\mathbf{z}_2\\\vdots\\\Delta\mathbf{z_N}\end{bmatrix} \tag{25}$$

and the matrices $\mathbf{h}$, $\mathbf{z}$ and $\Delta\mathbf{z}$ are defined as following

$$\mathbf{h}=\left[\sin\tau_1,\sin3\tau_1,...,\quad\sin\tau_2,\sin3\tau_2,...,\quad\cdots\quad\sin\tau_N,\sin3\tau_N,...\right] \tag{26}$$

$$\mathbf{z}=\left[b_{11},b_{12},...,\quad b_{21},b_{22},...,\quad\cdots\quad b_{N1},b_{NN},...\right]^T \tag{27}$$

$$\Delta\mathbf{z}=\left[\Delta b_{11},\Delta b_{12},...,\quad\Delta b_{21},\Delta b_{22},...,\quad\cdots\quad\Delta b_{N1},\Delta b_{NN},...\right]^T \tag{28}$$

Consequently, the initial solution of vectors $\dot{\mathbf{x}},\ddot{\mathbf{x}}$ and their increment $\Delta\dot{\mathbf{x}}$ and $\Delta\ddot{\mathbf{x}}$ are given by

$$\dot{\mathbf{x}}=\dot{\mathbf{H}}\mathbf{z},\ \ddot{\mathbf{x}}=\ddot{\mathbf{H}}\mathbf{z},\ \Delta\dot{\mathbf{x}}=\dot{\mathbf{H}}\Delta\mathbf{z},\ \Delta\ddot{\mathbf{x}}=\ddot{\mathbf{H}}\Delta\mathbf{z} \tag{29}$$

Using equations (20) and (24), the new solution of vector $\mathbf{z}_{new}$ are determined as

$$\mathbf{z}_{new} = \mathbf{z} + \Delta\mathbf{z} \tag{30}$$

Let the following matrices $\mathbf{K_{NL}(x)}$, $\frac{\partial}{\partial \mathbf{x}}\left[\mathbf{K_{NL}(x).x}\right]$, $\frac{\partial}{\partial \dot{\mathbf{x}}}\left[\mathbf{C_{NL}}\left(\omega_m \frac{\partial \mathbf{x}}{\partial \tau_m}\right).\frac{\partial \mathbf{x}}{\partial \tau_m}\right]$, $\mathbf{C_{NL}}\left(\omega_m \frac{\partial \mathbf{x}}{\partial \tau_m}\right)$, and $\frac{\partial \mathbf{x}}{\partial \omega_m}\left[\mathbf{C_{NL}}\left(\omega_m \frac{\partial \mathbf{x}}{\partial \tau_m}\right).\omega_m \frac{\partial \mathbf{x}}{\partial \tau_m}\right]$, simply denoted by $\mathbf{K_{NL}}$, $\mathbf{K_{NL}}1$, $\mathbf{C_{NL}}1$, $\mathbf{C_{NL}}$, and $\mathbf{C_{NL}}2$, respectively. Moreover, substituting equation (24) into equation (23) yields

$$\begin{aligned}
&\left[\sum_{m=1}^{N}\omega_m\left(\sum_{n=1}^{N}\omega_n\mathbf{M}\frac{\partial^2\mathbf{H}}{\partial\tau_m\partial\tau_n}+\left[\mathbf{C_L}+\mathbf{C_{NL}}\right]\frac{\partial\mathbf{H}}{\partial\tau_m}\right)+\left[\mathbf{K_L}+\mathbf{K_{NL}}1\right].\mathbf{H}\right].\Delta\mathbf{z}\\
&=-\left[\sum_{m=1}^{N}\omega_m\left(\sum_{n=1}^{N}\omega_n\mathbf{M}\frac{\partial^2\mathbf{H}}{\partial\tau_m\partial\tau_n}+\left[\mathbf{C_L}+\mathbf{C_{NL}}\right]\frac{\partial\mathbf{H}}{\partial\tau_m}\right)+\left[\mathbf{K_L}+\mathbf{K_{NL}}\right].\mathbf{H}\right].\mathbf{z}\\
&-\left[\sum_{m=1}^{N}\Delta\omega_m\left(\sum_{n=1}^{N}2\omega_n\mathbf{M}\frac{\partial^2\mathbf{H}}{\partial\tau_m\partial\tau_n}+\mathbf{C_L}.\left(\frac{\partial\mathbf{H}}{\partial\tau_m}\right)+\mathbf{C_{NL}}2\right)\right].\mathbf{z}
\end{aligned} \tag{31}$$

As a second step of the IHB method, solve equation (31) for the vector $\Delta\mathbf{z}$. This is performed by applying the Galerkin procedure.

$$\begin{aligned}
&\left(\int_0^{\tau_N}\cdots\int_0^{\tau_2}\int_0^{\tau_1}\left\{\mathbf{H^T}.\left[\sum_{m=1}^{N}\omega_m\left(\sum_{m=1}^{N}\omega_n\mathbf{M}\frac{\partial^2\mathbf{H}}{\partial\tau_m\partial\tau_n}+\left[\mathbf{C_L}+\mathbf{C_{NL}}1\right]\frac{\partial\mathbf{H}}{\partial\tau_m}\right)\right.\right.\right.\\
&\left.\left.\left.+\left[\mathbf{K_L}+\mathbf{K_{NL}}1\right].\mathbf{H}\right]\right\}.\mathbf{d}\tau_1\mathbf{d}\tau_2\cdots\mathbf{d}\tau_N\right).\Delta\mathbf{z}\\
&=-\left(\int_0^{\tau_N}\cdots\int_0^{\tau_2}\int_0^{\tau_1}\left\{\mathbf{H^T}.\left[\sum_{m=1}^{N}\omega_m\left(\sum_{m=1}^{N}\omega_n\mathbf{M}\frac{\partial^2\mathbf{H}}{\partial\tau_m\partial\tau_n}+\left[\mathbf{C_L}+\mathbf{C_{NL}}\right]\frac{\partial\mathbf{H}}{\partial\tau_m}\right)\right.\right.\right.\\
&\left.\left.\left.+\left[\mathbf{K_L}+\mathbf{K_{NL}}\right].\mathbf{H}\right]\right\}.\mathbf{d}\tau_1\mathbf{d}\tau_2\cdots\mathbf{d}\tau_N\right).\mathbf{z}\\
&-\left(\int_0^{\tau_N}\cdots\int_0^{\tau_2}\int_0^{\tau_1}\left\{\mathbf{H^T}.\left[\sum_{m=1}^{N}\Delta\omega_m\left(\sum_{m=1}^{N}2\omega_n\mathbf{M}\frac{\partial^2\mathbf{H}}{\partial\tau_m\partial\tau_n}+\mathbf{C_L}\frac{\partial\mathbf{H}}{\partial\tau_m}\right)\right.\right.\right.\\
&\left.\left.\left.+\mathbf{C_{NL}}2\right]\right\}.\mathbf{d}\tau_1\mathbf{d}\tau_2\cdots\mathbf{d}\tau_N\right).\mathbf{z}
\end{aligned} \tag{32}$$

Equation (32) can be rewritten in a simple form of a linear algebraic matrix equation system for unknown vector $\Delta\mathbf{z}$ as follows:

$$\mathbf{A}.\Delta\mathbf{z} = \mathbf{R} - \sum_{m=1}^{N}\Delta\omega_m.\mathbf{Q}_m \tag{33}$$

The matrix $\mathbf{A}$ is composed from linear and non-linear part:

$$\mathbf{A} = \mathbf{A_L} + \mathbf{A_{NL}} \tag{34}$$

where

$$\mathbf{A_L} = \int_0^{\tau_N} \cdots \int_0^{\tau_2} \int_0^{\tau_1} \left[\sum_{m=1}^{N} \omega_m \left(\sum_{n=1}^{N} \omega_n \mathbf{H^T M} \frac{\partial^2 \mathbf{H}}{\partial \tau_m \partial \tau_n} + \mathbf{H^T C_L} \frac{\partial \mathbf{H}}{\partial \tau_m} \right) + \mathbf{H^T K_L H} \right] . \mathbf{d}\tau_1 \mathbf{d}\tau_2 \cdots \mathbf{d}\tau_N \tag{35}$$

is the linear part and

$$\mathbf{A_{NL}} = \int_0^{\tau_N} \cdots \int_0^{\tau_2} \int_0^{\tau_1} \left[\sum_{n=1}^{N} \omega_n \mathbf{H^T C_{NL1}} \frac{\partial \mathbf{H}}{\partial \tau_m} + \mathbf{H^T K_{NL1}} \right] . \mathbf{d}\tau_1 \mathbf{d}\tau_2 \cdots \mathbf{d}\tau_N \tag{36}$$

is the non-linear part of the matrix **A** and the matrix **R** is given by

$$\mathbf{R} = \int_0^{\tau_N} \cdots \int_0^{\tau_2} \int_0^{\tau_1} \mathbf{H^T F} \mathbf{d}\tau_1 \mathbf{d}\tau_2 \cdots \mathbf{d}\tau_N - \mathbf{A_L} \cdot \mathbf{z} + \mathbf{R_{NL}} \tag{37}$$

where

$$\mathbf{R_{NL}} = -\left(\int_0^{\tau_N} \cdots \int_0^{\tau_2} \int_0^{\tau_1} \left[\sum_{m=1}^{N} \omega_m \mathbf{H^T C_{NL}} \frac{\partial \mathbf{H}}{\partial \tau_m} + \mathbf{H^T K_{NL} H} \right] . \mathbf{d}\tau_1 \mathbf{d}\tau_2 \cdots \mathbf{d}\tau_N \right) . \mathbf{z} \tag{38}$$

is the non-linear part of the matrix **R**.

Likewise, the matrix $\mathbf{Q}_m$ decomposed into linear $\mathbf{Q_{mL}}$ and non-linear part $\mathbf{Q_{mNL}}$ as follows:

$$\mathbf{Q_{mL}} = -\left(\int_0^{\tau_N} \cdots \int_0^{\tau_2} \int_0^{\tau_1} \left[\sum_{m=1}^{N} 2\omega_n \mathbf{H^T M} \frac{\partial^2 \mathbf{H}}{\partial \tau_m \partial \tau_n} + \mathbf{H^T C_L} \frac{\partial \mathbf{H}}{\partial \tau_m} \right] . \mathbf{d}\tau_1 \mathbf{d}\tau_2 \cdots \mathbf{d}\tau_N \right) . \mathbf{z} \tag{39}$$

$$\mathbf{Q_{mNL}} = -\left(\int_0^{\tau_N} \cdots \int_0^{\tau_2} \int_0^{\tau_1} \left[\mathbf{H^T} \frac{\partial}{\partial \omega_m} \left[\mathbf{C_{NL}} \left(\omega_m \frac{\partial \mathbf{x}}{\partial \tau_m} \right) . \omega_m \frac{\partial \mathbf{x}}{\partial \tau_m} \right] \right] . \mathbf{d}\tau_1 \mathbf{d}\tau_2 \cdots \mathbf{d}\tau_N \right) . \mathbf{z} \tag{40}$$

The matrices **h**, **z** and $\Delta\mathbf{z}$ can be defined from equations (26), (27) and (28) with two degree of freedom, $N = 2$. The solution starts by assuming initial values of vector **z**. Then matrices **A** and **R** are computed using equations (34) and (37), respectively. Thus, the unknown vector $\Delta\mathbf{z}$ is computed from equation (33) at constant frequency ω ($\Delta\omega = 0$). Once $\Delta\mathbf{z}$ is known, the new solution $\mathbf{z}_{new}$ is obtained by means of equation (30). This process is repeated iteratively using the Newton-Raphson procedure until the convergent solution is reached. Finally, the vector **x** can be obtained from equation (24).

3.2 Primary impact of the extendable smart front-end structure

Once again, to predict the behaviour of a vehicle with the extendable smart front-end structure involved in barrier offset frontal impact, the mathematical model shown in

Figure 4 is used to obtain the dynamic response of smart vehicles. The equations of motion of the give system are written as following equations.

$$M.\ddot{x} + F_{s1}(\delta_1) + F_{s2}(\delta_2) = 0 \tag{41}$$

$$m_C.\ddot{x}_C + F_{d1}(v_{d1}) + F_{d2}(v_{d2}) - F_{s1}(\delta_1) - F_{s2}(\delta_2) = 0 \tag{42}$$

$$I_b.\ddot{\theta}_b - F_{d1}(v_{d1}).l_b = 0 \tag{43}$$

$$I_C.\ddot{\theta}_C + \left[\left(F_{d1}(v_{d1}) - F_{s1}(\delta_1)\right].l_b = 0\right. \tag{44}$$

The deformations of the plastic springs are defined as equation (7) and the velocities of the hydraulic cylinders are given by

$$v_{d1} = \dot{x}_1 - \dot{x}_{C1},\ v_{d2} = \dot{x}_2 - \dot{x}_{C2} \tag{45}$$

where the displacements of the springs' ends x_1 and x_2 are defined as follows:

$$x_1 = x_C + l_b.\tan\theta_C,\ x_2 = x_C \tag{46}$$

The displacements of the dampers' ends x_{C1} and x_{C2} are given by

$$x_{C1} = l_b \tan\theta_b, x_{C2} = 0 \tag{47}$$

and the velocities of the springs' ends $\dot{x}_1$ and $\dot{x}_2$, as well as the velocities of the dampers' ends $\dot{x}_{C1}$ and $\dot{x}_{C2}$ are determined by differentiating equations (46) and (47), respectively as follows:

$$\dot{x}_1 = \dot{x}_C + l_b.\sec^2\theta_C.\dot{\theta}_C,\ \dot{x}_2 = \dot{x}_C \tag{48}$$

$$\dot{x}_{C1} = l_b \sec^2\theta_b.\dot{\theta}_b,\ \dot{x}_{C2} = 0 \tag{49}$$

Substituting equations (1), (2), (7), (45) to (49) into equations (41) to (44) yields

$$M.\ddot{x} + k_1.(x - x_C - l_b.\tan\theta_C) + k_2.(x - x_C) = F_1 \tag{50}$$

$$\begin{aligned} &m_C.\ddot{x}_C + c_1.\left(\dot{x}_C + l_b\sec^2\theta_C\dot{\theta}_C - l_b\sec^2\theta_b\dot{\theta}_b\right) + c_2.\dot{x}_C \\ &-k_1.(x - x_{C2} - l_b.\tan\theta_C) - k_2.(x - x_C) = F_2 \end{aligned} \tag{51}$$

$$I_b.\ddot{\theta}_b - c_1.\left(\ddot{x}_c + l_b\sec^2\theta_C\dot{\theta}_C - l_b\sec^2\theta_b\dot{\theta}_b\right)l_b = F_3 \tag{52}$$

$$I_C.\ddot{\theta}_C + c_1.\left(\dot{x}_c + l_b\sec^2\theta_C\dot{\theta}_C - l_b\sec^2\theta_b\dot{\theta}_b\right)l_b - k_1.(x - x_C - l_b.\tan\theta_C)l_b = F_4 \tag{53}$$

Equations (50) to (53) can be rewritten in the matrix form as equation (13) with $\mathbf{C_L}$, $\mathbf{C_{NL}}$, $\mathbf{KL}$, $\mathbf{K_{NL}}$, $\mathbf{F}$ matrices as follows:

$$\mathbf{C_L}=\begin{bmatrix}0 & 0 & 0 & 0\\ 0 & c_1+c_2 & 0 & 0\\ 0 & -c_1.l_b & 0 & 0\\ 0 & c_1.l_b & 0 & 0\end{bmatrix},\ \mathbf{C_{NL}}=\begin{bmatrix}0 & 0 & 0 & 0\\ 0 & 0 & -c_1.l_b.(S\theta)_b & c_1.l_b.(S\theta)_C\\ 0 & 0 & c_1.l_b^2.(S\theta)_b & -c_1.l_b^2.(S\theta)_C\\ 0 & 0 & -c_1.l_b^2.(S\theta)_b & c_1.l_b^2.(S\theta)_C\end{bmatrix}$$

$$\mathbf{K_L}=\begin{bmatrix}k_1+k_2 & -(k_1+k_2) & 0 & 0\\ -(k_1+k_2) & k_1+k_2 & 0 & 0\\ 0 & 0 & 0 & 0\\ -k_1.l_b & k_1.l_b & 0 & 0\end{bmatrix},\ \mathbf{K_{NL}}=\begin{bmatrix}0 & 0 & 0 & -k_1,l_b.\bar{\theta}_C\\ 0 & 0 & 0 & k_1,l_b.\bar{\theta}_C\\ 0 & 0 & 0 & 0\\ 0 & 0 & 0 & k_1,l_b^2.\bar{\theta}_C\end{bmatrix} \tag{54}$$

$$\text{and } \mathbf{F}=\begin{bmatrix}F_{01}+F_{02}-f_{01}-f_{02}\\ -F_{01}-F_{02}+f_{01}+f_{02}+F_{d1}+F_{d2}\\ -F_{d1}.l_b\\ (f_{01}+F_{d1}-F_{01}).l_b\end{bmatrix}$$

where $\bar{\theta}_C$ and $(S\theta)_C$ can be expressed as equations (15) and (16), respectively. Using the solution process discussed above, the vector **x** can be obtained from equation (24).

3.3 Secondary impact

The mathematical models shown in Figure 2 to Figure 4 are also used to define the interaction between the occupant and the vehicle body. The analysis of the vehicle/occupant impact dynamics is carried out in this section. To obtain the dynamic response of the occupant during the secondary impact, the equation of motion of the occupant is developed as follows:

$$m_o\ddot{x}_o+F_{so}(\delta_o)+F_{do}(v_o)=0 \tag{55}$$

where the deformation of the spring and the velocity of the damper of the occupant are defined respectively as

$$\delta_o=x_o-x,\ v_o=\dot{x}_o-\dot{x} \tag{56}$$

Substituting equations (3), (4), and (56) into equation (55) yields

$$m_o.\ddot{x}_o+c.\dot{x}_o+k.x_o=f(t) \tag{57}$$

where

$$f(t)=c(\dot{x}+v_{oc})+k(x+\delta_{oc}) \tag{58}$$

The general solution of equation (57) is determined in the following

$$x_o=e^{-\xi_o\omega_o t}(a\sin\omega_{do}t)+\frac{1}{m_o\omega_{do}}\int_o^t f(\tau)e^{-\xi_o\omega_o(t-\tau)}\sin\omega_{do}(t-\tau)\mathrm{d}\tau \tag{59}$$

The occupant is subjected to the following initial conditions

$$x_o(0) = 0, \qquad \dot{x}_o(0) = v_o \tag{60}$$

Using the initial conditions of the occupant, equation (59) can be rewritten as

$$\begin{aligned} x_o = {} & e^{-\xi_o \omega_o t}\left(\frac{v_0}{\omega_{do}}\sin(\omega_{do}t)\right) + \frac{e^{-\xi_o \omega_o t}\sin(\omega_{do}t)}{m_o \omega_{do}}\int_o^t f(\tau)e^{\xi_o \omega_o \tau}\cos(\omega_{do}t)\,\mathrm{d}\tau \\ & - \frac{e^{-\xi_o \omega_o t}\cos(\omega_{do}t)}{m_o \omega_{do}}\int_o^t f(\tau)e^{\xi_o \omega_o \tau}\sin(\omega_{do}t)\,\mathrm{d}\tau \end{aligned} \tag{61}$$

where

$$\xi_o = \frac{c_o}{c_{co}}, \qquad c_{co} = 2m_o\omega_o \qquad \omega_{do} = \omega_o\sqrt{1-\xi_o^2} \tag{62}$$

The velocity and the deceleration of the occupant are obtained by differentiation of equation (61).

4 Simulations

In this section, the analysis developed in the former sections is verified by the presentation of the simulation results.

The injury severity criteria are used to interpret the results. The main injury severity criterion of interest in this research is the intrusion criterion, which denotes the deformation of the vehicle structure and its effects on the passenger compartment. The second injury criterion that has been considered is the deceleration level of the occupant which measured as the maximum deceleration pulse sustained by the occupant during the crash event.

The following data are used in the numerical solution. The mass of the vehicle is M = 1,500 kg and the mass of the bumper is m_b = 50 kg. The force-deformation characteristic for the longitudinal member is shown in Figure 5 with the following values: f_{0i} = 0, k_{i1} = 250 kN/m and k_{i2} = 450 kN/m with δ_i^* = 0.3 m. The damping coefficient c_{k1} is assumed to be 10 kN.s/m till $v_{dk}^* = 10$ m/s, and c_{k2} = 12.5 kN.s/m. Moreover, the mass of the occupant is m_o = 65.7 kg. The occupant's restraint characteristics of the seat belt and the airbag are represented by stiffness k_o = 98.1 kN/m with initial slack length δ_{oc} = 0.005 m and damping coefficient c_o = 50 % of the critical damping. The initial velocity of the vehicle and the occupant is v_0 = 13.33 m/s.

Vehicle-to-barrier offset frontal impact is generally accompanied by high intrusion and is usually more critical than vehicle-to-barriers full frontal impact. Two sets of simulation runs involving a vehicle and a rigid barrier in head-on collision are used. The first set (smart impact) involves a collision of the fixed smart vehicle with the rigid barrier (SM-B). The second set (standard impact) involves a collision of the standard vehicle with the rigid barrier (ST-B). The aim of this investigation is to demonstrate the performance of the fixed smart front-end structure in 50% offset barrier frontal impacts. The time-histories of longitudinal member deformation and the deceleration of the occupant are obtained from the simulations. Figure 8 clearly shows the impacted side of

the smart vehicle's longitudinal member is deformed by 0.68 m, compared to 0.78 m of the standard vehicle. The result of the second injury criterion, deceleration of the occupant, is depicted in Figure 9. It shows that the smart vehicle's occupant sustains lower deceleration (28 g) while in the standard collision; the occupant suffers more deceleration (33 g).

Figure 8 Deformation of the front-end structure (see online version for colours)

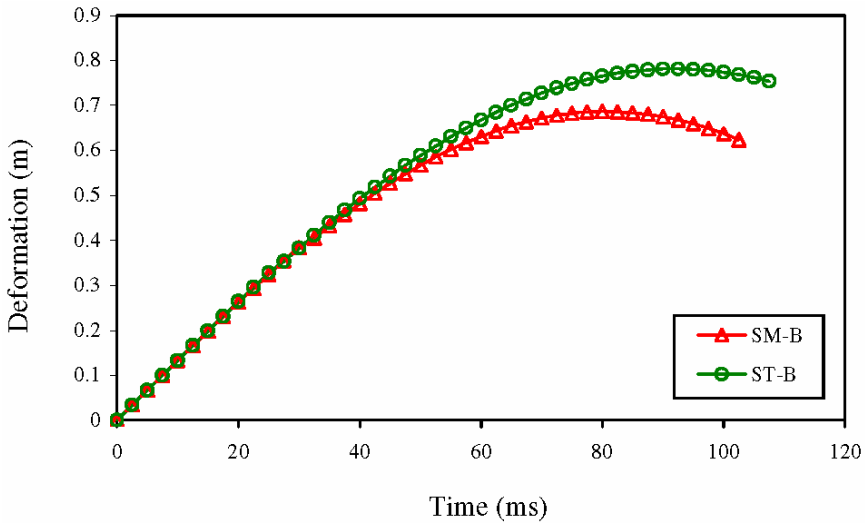

Note: Fixed smart front-end structure-to-rigid barrier offset impact.

Figure 9 Deceleration of the occupant (see online version for colours)

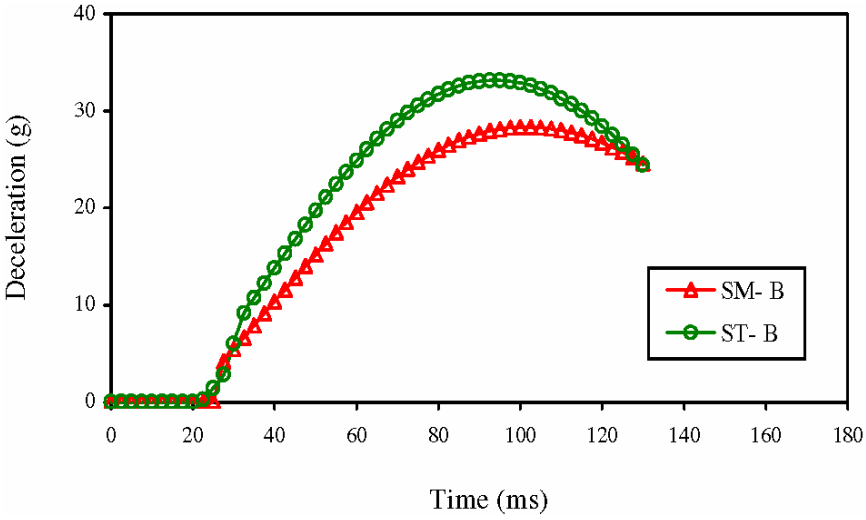

Note: Fixed smart front-end structure-to-rigid barrier offset impact.

Figure 10 Deformation of the front-end structure (see online version for colours)

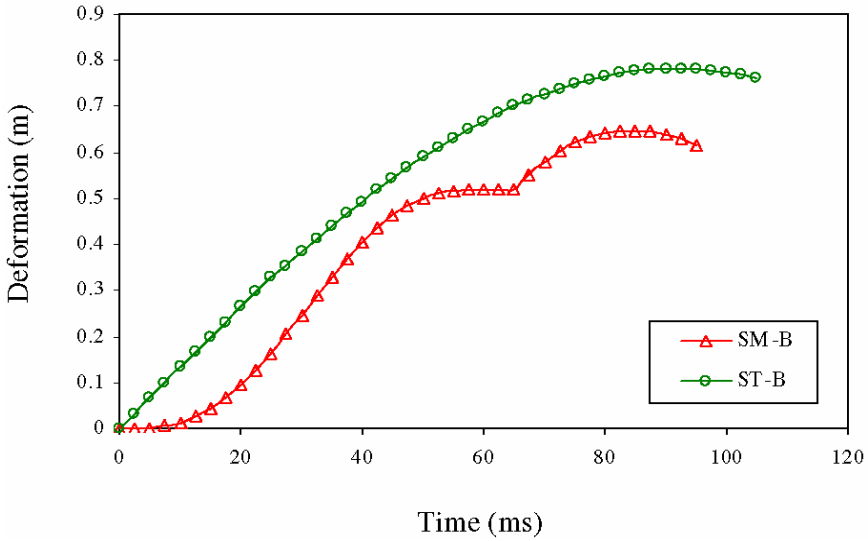

Note: Extendable smart front-end structure-to-rigid barrier offset impact.

Figure 11 Deceleration of the occupant (see online version for colours)

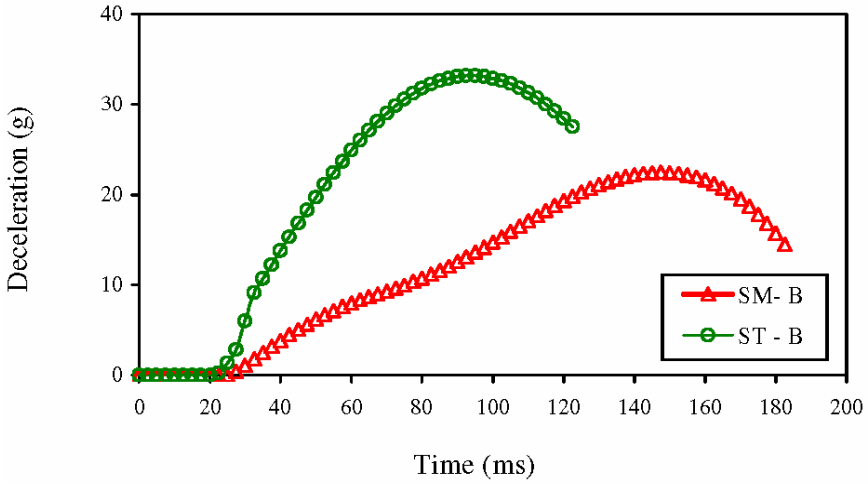

Note: Extendable smart front-end structure-to-rigid barrier offset impact.

The aim of the next investigation is to demonstrate the performance of the extendable smart front-end structure in 50% offset barrier frontal impacts. The time histories of the total deformation and the deceleration of the occupant, as obtained from the two simulations, are shown in Figure 10 and Figure 11, respectively. The reduction of the deformation is clearly shown in Figure 10. The longitudinal member of the standard vehicle is deformed by 0.78 m compared to 0.65 m of the smart vehicle. Furthermore, Figure 11 shows that the peak amplitude of the deceleration of the standard vehicle's

occupant appears to be about 33 g while the corresponding value of the smart vehicle's occupant is 22 g, which is considerably smaller.

5 Conclusions

In this paper, two types of smart front-end structures are studied to support the function of the existing vehicle structure. Mathematical models representing vehicle-to-rigid barrier offset frontal impacts for both types of smart front-end structures are introduced and analytical analysis using IHBM are developed. It is shown that the mathematical models are valid, flexible, and can be useful in optimisation studies. Furthermore, it is shown that IHB is an effective method to solve highly non-linear dynamical problems. It is proven from analytical simulations that development and analysis of mathematical models are efficient tools for predicting the dynamic response for offset frontal impacts. In addition, it is shown that the proposed structure concept surpasses the traditional structure concept in absorbing crash energy for the same crash distance and that brings significant improvements of both intrusion and deceleration injuries.

References

Appel, H. and Tomasd, J. (1973) 'The energy management structure for the Volkswagen ESV', SAE Paper No. 730078.

Chen, S., Cheung, Y. and Xing, H. (2001) 'Nonlinear vibration of plane structures by finite element and incremental harmonic balance method', *Journal of Nonlinear Dynamics*, Vol. 26, pp.87–104.

Clark, C. (1994) 'The crash anticipating extended airbag bumper system', *14th ESV Conference*, pp.1468–1480, Munich, Germany.

Ellis, E. (1976) 'Extensible vehicle bumper', US Patent Office, Pat. No. 3947061.

Elsholz, J. (1974) 'Relationship between vehicle front-end deformation and efficiency of safety belts during frontal impact', *5th ESV Conference*, pp.674–681, London, England.

Hiroyuki, M. (1990) 'A parametric evaluation of vehicle crash performance', SAE Paper No. 900465.

Hobbes, C. (1991) 'The need for improved structural integrity in frontal car impacts', *13th ESV Conference*, Paris, France, Paper No. S9-O-12, pp. 1073-1079.

Jawad, S. and Baccouch, M. (2001) 'Frontal offset crash-smart structure solution', *The ASME Mechanical Engineering Congress and Exposition*, pp.213–222, New York, NY, USA.

Jawad, S., Mahmood, H. and Baccouch, M. (1999) 'Smart structure for improving crashworthiness in vehicle frontal collisions', *The ASME Mechanical Engineering Congress and Exposition*, pp.135–144, Nashville, Tennessee, USA.

Lau, S. and Yuen S. (1993) 'Solution diagram of nonlinear dynamic systems by IHB method', *Journal of Sound and Vibration*, Vol. 167, pp.303–316.

Lau, S. and Zhang, W. (1992) 'Nonlinear vibrations of piecewise linear systems by incremental harmonic balance method', *Journal of Applied Mechanics*, Vol. 59, pp.153–160.

Lau, S., Cheuhng, Y. and Wu, S. (1982) 'A variable parameter incrementation method for dynamic instability of linear and nonlinear elastic systems', *Journal of Applied Mechanics*, Vol. 49, pp.849–853.

Lau, S., Cheuhng, Y. and Chen, S. (1989) 'An alternative perturbation procedure of multiple scales for nonlinear dynamics systems', *Journal of Applied Mechanics*, Vol. 56, pp.667–675.

Lau, S., Cheuhng, Y. and Wu, S. (1983) 'Incremental harmonic balance method with multiple time scales for periodic vibration of nonlinear systems', *Journal of Applied Mechanics*, Vol. 50, pp.871–876.

Lau, S., Cheuhng, Y. and Wu, S. (1984) 'Nonlinear vibration of thin elastic plates', *Journal of Applied Mechanics*, Vol. 51, pp.845–851.

Mizuno, K., Umeda, T. and Yonezawa, H. (1997) 'The relation between car size and occupant injury in traffic accidents in Japan', SAE Paper No. 970123.

Namuduri, G., Peruski, L. and Jones, G. (2004) 'Extendable bumper system and method of control', US Patent Office, Pat No. 6709035.

Pun, D. and Liu, Y. (2000) 'On the design of the piecewise linear vibration absorber', *Journal of Nonlinear Dynamics*, Vol. 18, pp.393–413.

Reuber, G. and Braun, A. (1994) 'Bumper system having an extendable bumper for automotive vehicles', US Patent Office, Pat No. 5370429.

Rupp, W. (1974) 'Front energy management parametric variation study', *5th ESV Conference*, pp.602–614, London, England.

Schwarz, R. (1971) 'Hydraulic energy absorption systems for high-energy collisions', *2nd ESV Conference*, Section 3, pp.36–74, Sindelfingen, Germany.

Wang, J. (1994) 'Bumper energy absorber', US Patent Office, Pat No. 5967573.

Witteman, W. (1999) 'Improved vehicle crashworthiness design by control of the energy absorption for different collision situations', PhD thesis, Eindhoven University of Technology, Automotive Engineering & Product Design Technology, Eindhoven, The Netherlands.

Witteman, W. and Kriens, R. (1998) 'Modeling of an innovative frontal car structure: similar deceleration curves at full overlap, 40 percent offset and 30 degrees collisions', *16th ESV Conference*, pp.194–212, Windsor, Ontario, Canada.

Witteman, W. and Kriens, R. (2001) 'The necessity of an adaptive vehicle structure to optimize deceleration pulses for different crash velocities', *17th ESV Conference*, pp.1–10, Amsterdam, The Netherlands.